Study of electron transport in nail-wire targets using the Vulcan Petawatt laser

T. Ma*, J. A. King, M. S. Wei and F. N. Beg
Department of Mechanical and Aerospace Engineering, University of California, San Diego, 9500 Gilman Drive, La Jolla, CA 92093, USA

R. J. Mason
Research Applications Corporation, Los Alamos, NM 87544, USA

M. H. Key, A. G. MacPhee, S. P. Hatchett, A. J. Mackinnon and P. K. Patel
Lawrence Livermore National Laboratory, P. O. Box 808, Livermore, CA 94550, USA

R. B. Stephens and K. U. Akli
General Atomics, P. O. Box 86508, San Diego, CA 92186, USA

R. R. Freeman, K. Highbarger, R. L. Weber and L. D. Van Woerkom
Department of Physics, The Ohio State University, 191 W. Woodrull Ave., Columbus, OH 43210, USA

J. S. Green, K. L. Lancaster, J. Pasley# and P. A. Norreys
Central Laser Facility, STFC, Rutherford Appleton Laboratory, HSIC, Didcot, Oxon OX11 0QX, UK

P. Jamangi and W. Theobald
Laboratory of Laser Energetics, University of Rochester, 250 East River Road, Rochester, NY 14623, USA

Contact | tyma@ucsd.edu

*Also at Lawrence Livermore National Laboratory, P.O. Box 808, Livermore, CA 94550, USA

#Also at the Department of Physics, University of York, Heslington, YO10 5DD, UK

Introduction

Understanding energy coupling and energy transport by relativistic fast electrons generated by ultra-intense laser-plasma interactions is fundamental to the fast ignition concept.[1]

In the cone-guided fast ignitor scheme,[2] a hollow reentrant cone inserted directly into the pre-compressed spherical fuel helps to guide the short-pulse laser to create energetic electrons at the cone tip. These hot electrons must then propagate through the 'overdense corona' surrounding the fuel core to spark ignition in the dense center. Thus, collimation of this beam of electrons and the distance over which the transport occurs are critical issues.

However, the physics of laser energy deposition and fast electron transport is difficult to diagnose in cones alone, and the use of a cone interface with a wire adds additional complexity in the joint between the wire and the cone.[3,4,5] Thus, a nail-wire target[6,7] was proposed consisting of a 1 mm long, 20 μm diameter copper wire drawn directly from an 80 μm hemispherical head. The motivation behind this simple, low-mass target was: i) to diagnose emission from the target from various angles and ii) to benchmark experimental data against hybrid PIC code much closer to experimental conditions spatially and temporally.

Experimental setup

The Vulcan Petawatt laser generated pulses at 1054 nm with durations of 1 ps with an on-target energy of approximately 350 J in a 7 μm FWHM focal spot, for a peak laser intensity of 3×10^{20} Wcm^{-2}. The target geometry and diagnostic configurations are shown in figure 1.

Three different diagnostics were simultaneously fielded to measure the Cu Kα emission from the target. The Cu Kα radiation at 8048 eV is predominantly due to binary collisions of the hot electrons with Cu ions, and thus its intensity is assumed to be proportional to the number of fast electrons.[8]

A Cu Kα Bragg reflection crystal imager[9] gave 2D time-integrated spatial information by detecting X-ray radiation within a narrow bandwidth around 8048 eV. The imager consisted of a SiO_2 2131 spherical quartz crystal with a radius of curvature of 38 cm, placed 20 cm from the target. The crystal operates 1.3° off axis in second diffraction order and with 15× magnification imaging onto a Fujifilm BAS-SR image plate. Resolution of the imager was approximately 20 μm. The view angle was in the horizontal plane at 29.4° from the nail-wire axis.

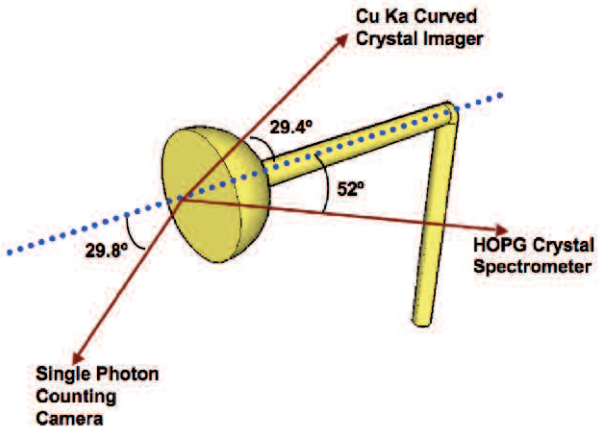

Figure 1. Layout of experimental setup showing diagnostic view angles relative to the nail-wire target axis.

The HOPG (highly oriented pyroltic graphite) Bragg crystal spectrometer[10] provided a spectrum of X-ray radiation with its randomly distributed scattering planes.

The crystal reflected x-rays over a 3.5 keV spectral bandwidth (centered about 8048 eV), with a spectral resolution of 5 eV, at a 52° view angle on the rearside of the nail-wire axis. The crystal was located 25 cm from both the X-ray source and the imaging plane. The spectrum was also recorded on Fujifilm BAS-SR image plates.

The single photon counting camera [11] had a CCD camera configured such that no more than one photon hit each CCD pixel, so that the CCD counts were proportional to photon energy and the data could give an absolute measure of K-shell radiation emission. A Spectral Instruments Series 800 CCD with a pixel size of 13.5 μm, and a 2048 × 2048 pixel array recorded spectra through a 150 μm Cu filter. The CCD was positioned 380 cm from TCC, with a front view of 29.8° to the nail-wire axis.

By comparing all three of these Cu Kα diagnostics, and using the strengths of each (the accurate relative line strengths of the HOPG, and the absolute accuracy of the single photon counting camera), a cross-calibration was completed by J. A. King, *et al.* [4] in which an absolute number of Kα yield was taken from single photon counting exposures by summing the number of pixels contained in the Kα peak. CCD quantum efficiency, single hit probability, filter attenuation and solid angle subtended by the detecting surface, as well as diagnostic view angle and opacities were accounted for to give total Cu Kα/sr emitted in the direction of the single photon counting camera. Relative Kα line intensities from the HOPG were integrated, background subtracted and opacity corrected to give a total Kα count. The HOPG was then normalized against the associated absolute Kα yields from the single photon counting camera. This methodology was applied to several shots on Cu targets in a similar configuration as the nail-wire targets to produce a trend line, and Kα yields were corrected to the line value. These yields were then compared against the signals from the Cu Kα imager. A scaling factor of $(5.1\pm0.9)\times10^{-6}$ Kα/sr/μm per PSL (PhotoStimulated Luminescence – values read out by the image plate scanner) was then derived for associated Kα levels corresponding to counts on the image plates.

Experimental results

Figure 2 illustrates the intense emission seen from the nail head and the subsequent transport down the wire as displayed by the Cu Kα crystal imager. The Kα imager displays bright emission from the nail head and exponential fall off of brightness along the wire, showing that the majority of the Kα production and the highest temperatures occur in the head.

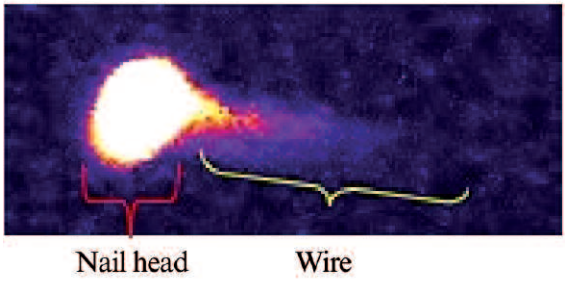

Figure 2. Cu Kα emission from the nail-wire target.

Absolute Kα yields were determined for the wire portion of the nail-wire target. Because the physics of the hot electron transport within the nail head was difficult to deconvolve due to its hemispherical geometry and ambiguities in the pattern of energy deposition within it, only the electron transport within the wire itself was considered.

Absolute Kα yields were then determined for the wire portion of the nail-wire target based on the Cu Kα crystal image. A lineout integrated transversely along the wire axis was corrected for view angle and opacity. It was assumed that the Kα energy density was homogeneous within a radial cross-section of the wire, and the 22.3 μm attenuation length of 8048 eV radiation in copper was accounted for in the line-of-sight opacity correction.

The hot electron transport was modeled using a 1D resistive transport numerical code. [12] The model assumed a Maxwellian-Boltzmann distribution of hot electrons injected axially into the wire (the propagation distance through the head was ignored). In small increments along the wire, the code calculated the conversion of electron kinetic energy to Kα X-ray and to thermal energy. The modeled Kα profile was matched to the experimental axial emission profile (corrected for view angle and opacity) by varying the simulation input parameters of injected laser energy (i.e. coupling efficiency) and average initial hot electron temperature (T_{hot}).

The simulation also scaled the Kα profile accordingly for imager reflectivity. In practice, the Kα spectral line tends to shift and broaden with increasing temperature, and thus, can shift off the narrow bandwidth (~6 eV) of the Cu Kα crystal. [12] The collection efficiency of the Cu Kα crystal was thus dependent on the temperature of the target, and corrections needed to be made for the potential loss in signal due to it. By using the population kinetics model FLYCHK, Akli *et al.* [12] showed that the collection efficiency of the Kα imager steeply drops to ~25% between 0 and 20 eV. However, an added benefit of this effect is that because the imager is so sensitive to temperature, the reduction in collected Kα photons can be calculated and used as an average temperature diagnostic.

The absolute Kα emission (proportional to the hot electron current) had a peak intensity of 3.2×10^{-6} J/sr/μm at the start of the wire, and an exponential fall off of approximately 80 μm scale length along the wire. The higher temperatures found at the initiation of the wire require a larger yield adjustment which leads to the steepening of the profile seen in the temperature-corrected profile. At 200 μm along the wire, the emission has fallen nearly an order of magnitude to 3.52×10^{-7} J/sr/μm.

Based on the 1D code, the laser energy converted into electrons down the wire was approximately 1.7 J. With an initial injection laser energy of 350 J, this gave a coupling efficiency into hot electrons, η, of approximately 0.5%. It is of interest to note that this value is the energy coupled into just the wire; obviously, as evidenced by the raw Kα images, considerable energy was deposited within the nail head itself. The fitting of the numerical code to the data gave a Thot electron temperature of approximately 600 keV.

These results were also compared against Bell *et al.'s* 1D analytic resistive transport model,[13] which requires the thermal return current to be everywhere equivalent and charge-neutralizing against the hot electron current in order for energetic electrons to propagate. In this model, hot electron collisional losses were neglected, and conductivity was constant at $10^6\ \Omega^{-1}m^{-1}$. Fitting to this model predicted an expected hot electron penetration scale length of approximately 125 μm.

The shorter measured experimental penetration distance compared to the Bell model prediction is evidence of inhibition of the fast electron transport due to electric fields. The reduced electron range thus gives an incorrectly low Kα estimate of the hot electron temperature. This decay of emission is consistent with bulk Ohmic inhibition of the hot electron transport.

Figure 3 marks the experimental profile, the fit using the 1D transport code, the adjusted profile when the temperature shift of the Kα line is taken into account, and the predicted analytical profile.

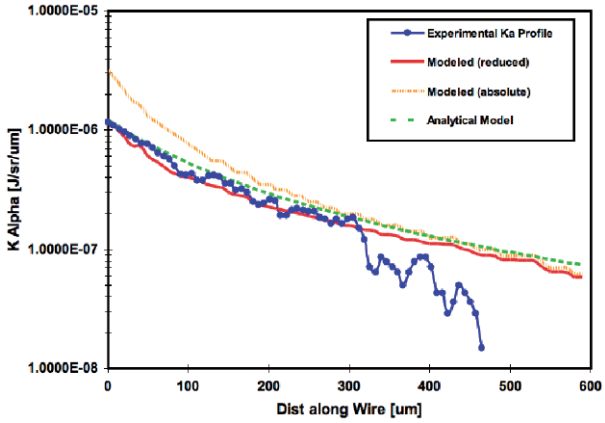

Figure 3. Experimental, 1D numerically modeled, and analytically predicted profiles of Kα/sr/μm for the nail-wire.

Modeling and discussion

The e-PLAS simulation code based on moment/hybrid techniques[14] was used to model the transport of the relativistic electrons in these nail-wire targets.[15] Hot electrons driven by the laser (flat pulse in planar polarization at normal incidence) were generated at ponderomotive potential energies as predicted by Wilks[16] (in this case, γ=10.3) and were launched normally on the nail head. The target material was modeled as copper with an average effective atomic number of Z=15. The mesh was Cartesian, and the target was modeled with a 100 μm head and a wire diameter of 20 μm. Hot electrons were stopped by drag against the background cold electrons, and by self-consistent E-fields arising from the resistance of the cold background returning to maintain charge neutrality.

The code showed that hot electrons tend to remain trapped in the head and accumulate brightly near the edges of the laser spot. Jets of hot electrons ran nearly vertically toward the head edges as well as axially down the wire. Resistive heating was the most dominant mechanism and predicted B fields are most intense near the head, where they exceed 300 MG.

Furthermore, e-PLAS showed a peak n_h near the laser spot of order 2×10^{21} cm^{-3}. The hot density dropped to 10^{20} cm^{-3} at 200 μm into the wire. At 2 ps the colds in the wire at the 200 μm position were approximately 250 eV, whereas the cold temperature in the head was approximately three times greater, indicating far more energy was trapped in the head than made it down the wire. Figure 4 shows a density plot and a cold electron temperature profile as produced by e-PLAS.

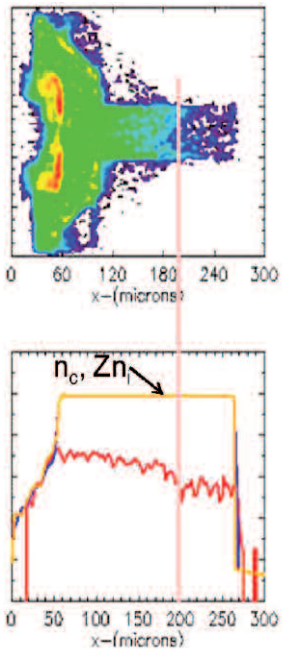

Figure 4. Density plot at 2 ps. The vertical line marks the depth at which the hot density has dropped an order of magnitude to 10^{20} cm^{-3}.

Conclusion

The relatively short penetration depth of the fluorescent emission along the length of the wire suggests Ohmic stopping consistent with the Bell model. Further, it has been found that a large portion of hot electrons are 'bottlenecked' within the nail head itself, and do not make it down the wire. The relatively low 0.5% coupling efficiency into the wire derived from the 1D numerical transport model is consistent with the large >300 MG B-fields seen in e-PLAS confining the majority of hot electrons to the nail head.

Acknowledgements

This work was performed under the auspices of the U.S. Department of Energy under contracts DE-AC52-07NA27344, W-7405-Eng-48 No. DE-FC02-04ER54789 (Fusion Science Center). The work and assistance of the technical, scientific and administrative staff associated with the Vulcan Laser Facility are gratefully acknowledged. T. Ma is funded under LLNL's Institute of Laser Science and Applications grant and the Lawrence Scholar Program.

References

1. M. Tabak *et al*., *Phys. Plasmas* **1**, 1626 (1994).
2. S. P. Hatchett and M. Tabak, *'Cone Focus Geometry for Fast Ignition,'* presented at 30th Annual Anomalous Absorption Conf. Ocean City, Maryland, April 2000; see also S. Hatchett *et al*., *'New Developments in Design of Cone-Focused Fast Ignition Targets,'* presented at 31st Annual Anomalous Absorption Conf., Sedona, Arizona, June 3-8, 2001.
3. R. Kodama *et al*., *Nature* **432**, 1005 (2004).
4. J. A. King *et al*., manuscript in preparation.
5. J. S. Green *et al*., *Nat Phys* **3**, 853-856 (2007).
6. J. Pasley *et al.*, *Phys. Plasmas* **14**, 120701 (2007).
7. M. Wei *et al*., manuscript in preparation.
8. S. Bastiani *et al*., *Phys. Rev. E*, **60**, 3439 (1999).
9. J. A. Koch *et al*., *Rev. Sci. Instrum*. **74**, 2130 (2003).
10. A. Pak *et al*., *Rev. Sci. Instrum.* **75**, 3747 (2004).
11. C. Stoeckl *et al*., *Rev. Sci. Instrum.* **75**, 3705 (2004).
12. K. U. Akli *et al*., *Phys. Plasmas* **14**, 023102 (2007).
13. A. R. Bell *et al.*, *Plasma Phys. Control Fusion* **39**, 653-659 (1997).
14. R. J. Mason *et al*., *IEEE Trans. Plasma Sci.* **PS-14**, 45 (1986).
15. R. J. Mason *et al*., ICOPS 2007 Proceeding (2007).
16. S. C. Wilks *et al*., *Phys. Rev. Lett.* **69**, 1383 (1992).